Microfluidics and Nanofluidics (2019) 23:102
https://doi.org/10.1007/s10404-019-2268-0

RESEARCH PAPER

Digital flow rate sensor based on isovolumetric droplet discretization effect by a three-supersurface structure

Xuan Li[1,2] · Yuxin Mao[1,2] · Zhicheng Zhu[1] · Yinghui Zhang[1,2] · Zecong Fang[3] · Dong Wu[1,2] · Hang Ding[1] · Tingrui Pan[3] · Baoqing Li[1,2] · Jiaru Chu[1,2]

Received: 10 January 2019 / Accepted: 23 July 2019

Abstract
Minute droplets play a growingly important role in the fields of manufacturing and measurement for the ability of being miniscule liquid carries. A digital microfluidic flow rate sensor, which works by counting the number of droplets generated between two electrodes, is designed and fabricated in this article. The droplets with equal volume ranging from nanoliter to microliter are generated by a three-supersurface structure (TSS), and the droplet volume is directly related to the size of gap in the TSS, which means that the resolution of the flow rate sensor can be simply tuned by changing the gap. A theoretical model is presented to reveal the mechanism of the isovolumetric discretization effect, showing that the superhydrophobicity/superhydrophilicity of the TSS's three surfaces plays the most important role in the isovolumetric droplet discretization. Both numerical simulation and experimental results demonstrate that the droplets can keep uniform size at different flow rates under 200 μL/min, indicating a potential application of the digital flow rate sensor for low rate metering in microfluidic devices.

Keywords Microfluidics · Droplet discretization · Flow rate · Digital flowmeter

1 Introduction

The discretization of liquid into droplets is an extensive phenomenon and plays growingly important roles in our life and research. For example, droplet microfluidics has provided a tool to encapsulate cells and reagents for biomedical applications, such as tissue engineering, high-throughput screening and cell bioreactors (Droplet Generation 2008; Ryoun Youn and Seok Song 2012; Wu et al. 2006). Specifically, droplet discretization in the murphy drip chamber of infusion apparatus is widely utilized in the clinic, which splits the drug solution into small drops for observation and estimation of the drip rate (Cataldo et al. 2012; Hillman 1989; Murphy 1909). Actually, the drip rate referring to the number of drops that enter the dripping chamber in a period of time is based on the assumption that each drop keeps constant in size at different remain volumes of the fluid (that is, at different pressures). However, the volume of each drop may change due to variation of fluid pressure during the drop infusion, leading to an inaccurate calculation of the infusion rate. It is because larger flow pressure could accelerate the separation and leads to smaller size droplet generation (Fig. S1).

Recently, some researchers have proposed a new kind of microfluidic digital flow rate sensor based on the discrete droplets. The digital droplet flow rate sensor is originated from Pan group (Heikenfeld et al. 2018; Yang et al. 2017). They developed a patterned fabric with distinct surface wettability to discrete the sweat into droplets, and then measured the flow rate by counting the number of droplets during a period of time. Based on similar sweat-sensing principle,

Xuan Li and Yuxin Mao have contributed equally to this work.

Electronic supplementary material The online version of this article (https://doi.org/10.1007/s10404-019-2268-0) contains supplementary material, which is available to authorized users.

✉ Baoqing Li
bqli@ustc.edu.cn

[1] School of Engineering Science, University of Science and Technology of China, Hefei 230027, Anhui, China

[2] Key Laboratory of Precision Scientific Instrumentation of Anhui Higher Education Institutes, University of Science and Technology of China, Hefei 230027, Anhui, China

[3] Department of Biomedical Engineering, University of California, Davis 95616, USA

Published online: 31 July 2019

the Gomez group (Francis et al. 2018) developed a prototype of sweat rate meter with in vivo demonstration. The results demonstrated the feasibility of digital droplet flow rate sensor for microfluidic devices application. The ability to create small monodisperse liquid droplets with uniform volume is of importance in constructing reliable flow rate sensor (Ben-Tzvi and Rone 2010). However, the uniformity of the generated droplets was seldom analyzed when the flow rate changed during the detection procedure. Bioinspired by lotus rims, Jiang group (Dong et al. 2013) has reported a droplet discretization method using a superhydrophobic nozzle. In that case, droplet volume was only determined by the inner size of the superhydrophobic-treated needle but only at a low velocity (in a quasi-stable state).

In this paper, we studied the droplet discretization effect at various flow rates and proposed a new type of liquid discretization method by a three-supersurface structure (TSS) which is capable of discretizing liquid isovolumetrically and reducing the droplet volume's dependence on the flow rate. The theoretical model and simulation analysis of the droplet discretization process have also been studied in detail to further analyze the relationship between discrete volume, flow rate and the spatial gap between the two superhydrophobic surfaces. Moreover, we implemented a preliminary trial on the digital droplet flow meter based on TSS, demonstrating the application on measuring liquid flow rates by tracking the frequency of droplet formation by TSS.

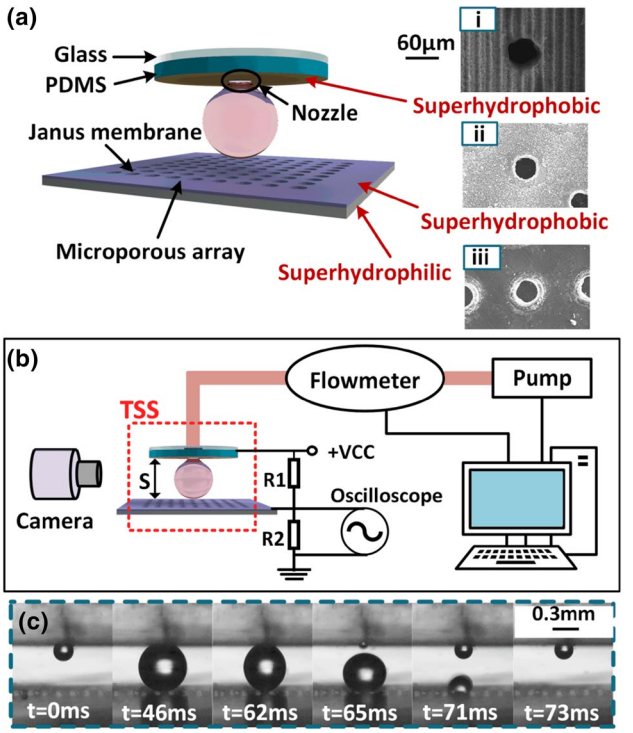

Fig. 1 **a** The schematic of the TSS and SEM photos (i, ii, iii) of three surface morphologies. The contact angles of water on the three surfaces are 154.5°, 150.3°, 17.2°, respectively. **b** A schematic of the experimental setup. **c** The screenshot recorded by a high-speed camera visualizes the process of the discretization effect by the TSS with the gap of 0.5 mm and flow rate of 50 μL/min

2 Methods

2.1 Fabrication process of the TSS

As shown in Fig. 1a, the TSS consists of two main parallel layers, between which there is a gap represented by S. The first layer has a superhydrophobic surface with a nozzle in the center for droplets outflow, and the second layer, a thin Janus membrane (Tian et al. 2014; Yun et al. 2017), has a microporous array for liquid to flow through. The TSS was fabricated using a superfast femtosecond laser direct-writing technology, which has been an ideal tool to fabricate combined micro- and nanostructures over different substrates (Wood et al. 2018; Yin et al. 2015; Yong et al. 2015). The fabrication process of the first layer is as follows: a 150 μm thick coverslip was bonded with a 254 μm thick polydimethylsiloxane (PDMS) membrane using oxygen plasma treatment; a through hole was fabricated on the glass-PDMS bonding material as a nozzle (60 μm in diameter) using a regenerative amplified Ti: sapphire femtosecond laser system (Coherent, Chameleon Vision-S/Legend Elite F HE-1K) with a speed of 10 mm/s, a pulse energy of 100 mW and a scanning cycle of 300 times; then, the laser was also used to treat the surface of PDMS material to obtain a superhydrophobic surface property (the water contact angel $\theta > 150°$) with laser pulse energy of 60 mW and scanning a grid pattern (Mao et al. 2018). The second layer was made up of an aluminum membrane with the thickness of 20 μm. A microporous array (4×4 mm^2 in area) with a diameter of 60 μm and a pitch of 200 μm was fabricated in the membrane using femtosecond laser with a power of 200 mW. Next, the film was immersed into 1H, 1H, 2H, 2H-perfluorodecyltriethoxysilane (PFDTES) solution at room temperature for 12 h, forming superhydrophobic surfaces on both sides of the aluminum membrane. Successively, the lower surface of the PFDTES-modified film was ablated by a femtosecond laser at a speed of 15 mm/s, a pulse energy of 70 mW and scanning spacing of 20 μm, to remove the fluorosilane coating on the lower surface and the inner wall of the microporous array. As a result, the lower surface and the inner wall became superhydrophilic, while the upper surface remained superhydrophobic. Finally, the two layers can be integrated parallelly with a certain gap distance, and two rubber tubes would be glued in the top and the bottom of TSS separately as inlet and outlet, respectively. In our experiment, we did not package the TSS as sealed device because of the convenience of investigating

the influence of different gap distance on the discretization effect. Instead, we fixed the first layer on a precision vertical shifting with the precision of ± 0.01 mm. It is certainly possible to imagine a device constructed with a package preventing contamination and evaporation during the process.

2.2 Experimental setup

A schematic of the experimental setup is shown in Fig. 1b. The fluid used is 99% DI water and 1% NaCl in mass. S, representing the distance between two superhydrophobic surfaces, is tuned by a manual stage (GCM-V13M, Daheng Optics), and the inlet flow rate is adjusted by a commercial microfluidic flow control system (MFCS™-EZ, Fluigent Company). The discrete droplet volume is measured in real time by the commercial flow rate platform (Fluigent Company) with the range of ± 1 mL/min and the accuracy of 15 µL/min. The frequency of discrete droplet is detected by the output signal of detection circuit and the process is supervised by a high-speed camera (CHRONOS 1.4, Kron Technologies Inc.).

2.3 Measurement method of the droplet volume

In the process of droplet discretization, the liquid is firstly extruded from the nozzle to form a droplet. Then, the droplet touches the second superhydrophobic surface and breaks under the action of Laplace force. As shown in Fig. 1b, an electric circuit was built to detect the contact conditions of droplet with the Janus membrane. When the droplet contacts the Janus membrane, a high-level voltage is detected; while after the droplet breaks and penetrates the Janus membrane quickly, a low-level voltage is detected. An oscilloscope (Rigol DS1022U) was used to acquire the pulse signal, which directly presented the period (t_p) and the frequency (f). Since the fluid is continuously transported at a constant flow rate, the volume of single droplet (V) can be calculated by multiplying flow rate (Q) and the time between two adjacent droplet discretization (that is, t_p). When the droplet was generated without the TSS, the number of the droplets n can be counted by a camera. The volume of the droplet can be calculated by $V = Q \cdot t/n = Q \cdot f$, where t is the total time of the droplet discretization.

3 Results and discussion

3.1 The effect of TSS on discrete droplet volume

The high-speed sequential images of a typical discretization process are illustrated in Fig. 1c. As can be seen, when the liquid begins to flow out of the nozzle ($t = 0$ ms), a spherical droplet forms and grows up gradually ($t = 46$ ms). Once the droplet grows large enough to contact the second layer ($t = 62$ ms), it is drawn by the suction force from the micropores and rapidly separated from the nozzle ($t = 65$ ms). The droplet passes through the microporous array ($t = 71$ ms) and then it is guided away by the superhydrophilic surface. As the droplet merges into the underside of the membrane, another droplet begins to form from the nozzle ($t = 73$ ms), and the process would repeat again. During the process, continuous flow is discretized into independent droplets in the gap by the TSS.

The wettability of each surface plays a crucial role in the isovolumetric droplet discretization. Firstly, the solid–liquid–gas contact line is confined to the circumference of the nozzle and its expansion is limited due to the natural characteristic of the superhydrophobicity (Cao et al. 2015; Dong et al. 2013). Secondly, the difference in wettability between the upper and lower surfaces of the second layer induces different water/air interface shapes of liquid, namely spherical at the upper surface and flat at the lower one. Then, a Laplace pressure is generated between the two surfaces to let liquid quickly drain off (in several milliseconds). In addition, the superhydrophobicity of the second surface has the ability to avoid residual liquids.

To explore the influence of the TSS on droplet formation, experiments were carried out with and without the TSS. When droplets separate from a superhydrophobic nozzle without the Janus membrane, the droplet volume decreases from 5.89 to 4.24 µL with flow rate increasing from 50 to 200 µL/min, as shown in Fig. 2a. The increase in the flow pressure induces a great decrement of the droplet volume. On the other hand, when the Janus membrane is parallelly assembled close to the nozzle at a space of 0.3 mm, the average droplet volume is dramatically decreased to 10.8 nL. Specifically, the droplet size varies only between 11.5 and 10.1 nL along with the change of flow rate from 50 to 200 µL/min with the TSS. Notably, the 20 µm thickness membrane was observed vibrating during the discretization process, which might be a significant reason for the slight variation of the droplet volume at high flow rates.

Furthermore, we explored the droplet separation with the gap at 0.3 mm, 0.5 mm, 1.0 mm and 2.0 mm of the TSS. In the experiments, we set flow rates of 50, 100 and 150 µL/min for each structure gap. As shown in Fig. 2b, the average volumes of droplet are 11.1 nL, 59.7 nL, 0.474 µL and 3.12 µL, which grow cubically as a function of the gap (S), with the fitting formula for experiment:

$$V_f = 0.218S^3 + 0.445S^2 - 0.220S + 0.031. \quad (1)$$

Meanwhile, the variations of droplet volume with flow rates are 0.341 nL, 1.08 nL, 22.8 nL and 99.8 nL, respectively. The smaller the gap, the smaller is the variance of the droplet's volume. It demonstrates that the TSS can discrete the continuous flow into isovolumetric droplets. In this case,

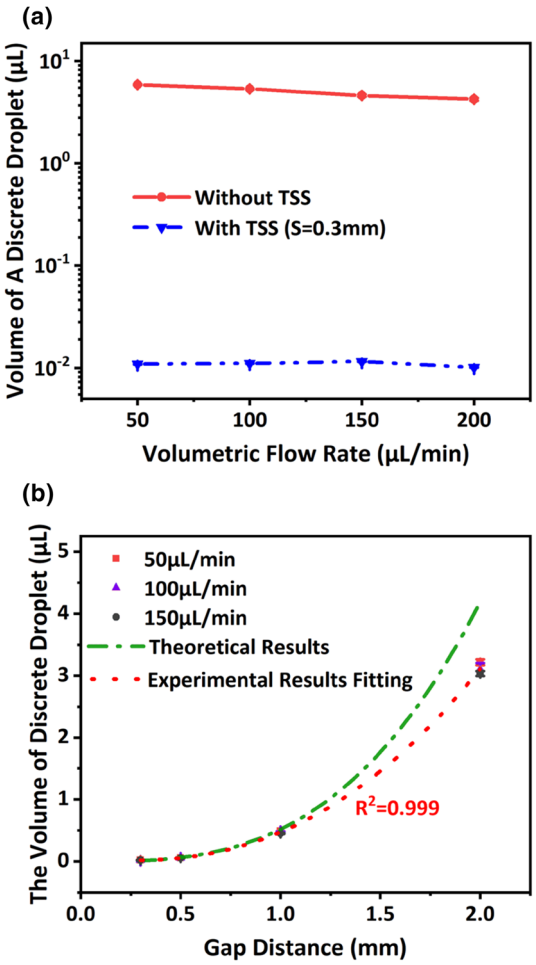

Fig. 2 **a** The experimental comparison of droplet sizes under different flow rates with and without the TSS. The red solid line represents the discrete volume generated only by a superhydrophobic nozzle, and the blue dash-dot-dot line represents droplet volume of the discretization by the TSS with a gap of 0.3 mm. **b** The relationship between single droplet volume and gap distance with the TSS. The red dot line and the green dash-dot line represent the fitting data of the experimental results and the theoretical results, respectively (color figure online)

the droplet size is basically dominated by the gap between two superhydrophobic surfaces.

3.2 Investigation on the discretization mechanism via TSS

3.2.1 The mathematical model

A mechanical model is established to analyze the mechanism of the droplet formation here. When a droplet is hanging at the nozzle as shown in Fig. 3a, the upward surface tension force $F_{\sigma y}$ is balanced with the sum of vertical gravitational force G and water pressure force F_{p} as

$$F_{\sigma}\sin\theta_{\mathrm{d}} = G + F_{\mathrm{p}}\,, \tag{2}$$

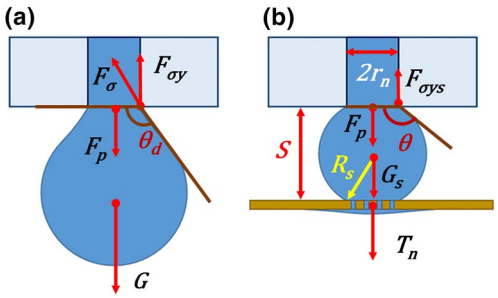

Fig. 3 Schematics of the mechanism analysis of droplet discretization: **a** without a Janus membrane, the detachment of droplet is dominated by gravity G; **b** discretization by the TSS with the gap S is dominated by Laplace force T_n

where θ_{d} is the droplet suspension angle. F_{p}, which has positive correlation with the volumetric flow rate of the liquid (Q) when Q is from 0 to 50 μL/min, can be described as $F_{\mathrm{p}}=f(Q)$ (shown in Fig. S5, derivation details can be found in Eqs. (S1–S8) in supplementary materials). The flow pressure F_{p} is constant under a fixed flow rate; thus, the gravity will increase with the droplet growing until the sum of gravity and the flow pressure exceeds the maximum surface tension, at which point droplet separation occurs. During this process, θ_{d} will decrease close to 90° (shown in Fig. S2) where the surface tension is at its maximum as $\pi\sigma D_{\mathrm{c}}$ (the σ and D_{c} are surface tension coefficient and the diameter of the water–air–solid contact line). Hence, the critical volume of the separated droplet is given by

$$V = \frac{\pi\sigma D_{\mathrm{c}} - f(Q)}{\rho g}. \tag{3}$$

From Eq. (3), it can be concluded that the volume of the discretized droplet has a noticeable tendency to decrease with increasing flow rate Q, which explains the experimental results shown in the Fig. 2a. A more specific verification of Eq. (3) is given in the supplementary materials in Sect. 4.

When a Janus membrane is placed close to the nozzle, the droplet will contact with the membrane in advance of droplet separation, as shown in the Fig. 3b. At this moment, gravitational force (G_{s}), upward surface tension force ($F_{\sigma y}$) and pressure force (F_{p}) are present. In addition, the suction force (T_n) is exerted on the droplet too, which is mainly caused by Laplace pressure force from wettability gradient of the Janus membrane. The suction force T_n acting on the droplet can be calculated according to Eq. (S12). In this case, Eq. (2) can be expressed as

$$F_{\sigma}\sin\theta < T_n + G_{\mathrm{S}} + F_{\mathrm{p}}. \tag{4}$$

Details of the derivation and analysis are given in the supplementary materials in Eqs. (S8–S12). Therefore, it is reasonable to believe that the suction force is the main factor causing the droplet discretization when using the TSS. As a

result, once the liquid touches the second superhydrophobic of the TSS, it would quickly break away from the nozzle and penetrate through the microporous array. In this case, the volume of droplet is mainly determined by the gap and should be independent of the variation of flow rate in theory. Consequently, here we focus on analyzing the mechanism of discretization in the vertical direction. The influence of the orientation of TSS on the volume of droplet is negligible because according to Eq. (4), it is found that in the experiment G_S is less than one-tenth of T_n. This conclusion can also be demonstrated by the calculated Bond number, which is 0.55, for the largest gap we tested ($S = 2$ mm). Hence, the droplet is sandwiched between two superhydrophobic surfaces and the volume is close to

$$V_S = \frac{\pi S^3}{6}. \tag{5}$$

It can be seen from Fig. 2b, where the green dot-dashed line representing the theoretical model matches the experimental results very well at gap of 0.3 mm and 0.5 mm. While at gaps larger than 1 mm, the error obviously enlarges. This is because the droplet is elongated at bigger gap and unable to be simplified as an ideal sphere at this moment. In conclusion, the TSS makes the droplet separate equally in volume under different flow rates, and the volume is controllable and predicable by a simple mathematic model.

3.2.2 The numerical simulation

A simulation model was also established using the diffuse interface immersed boundary (DIIB) (Chen et al. 2018; Liu and Ding 2015; Liu et al. 2017) method to further investigate the process of droplet formation and separation. Figure 4a shows the process of the droplet formation along with time (t). It can be observed that the simulated result of discretization process (Movie S1) is morphologically consistent with the real process recorded by the high-speed camera (Fig. 1c). Also, the simulation shows that the time from droplet contacting with the Janus membrane to breaking from the nozzle is quite fast in approximately 6 ms.

Furthermore, we simulated discretization process under different flow rates. The simulation results reflecting the variation trends of discrete liquid volumes in various flow rates and different gap distances are shown in Fig. 4b. As the gap was set at 0.5 mm, 0.3 mm, 0.2 mm, the average volume of single droplet was 62.1 nL, 12.9 nL, 3.15 nL, and the volume variance of single droplet was 2.7 nL, 1.1 nL, and 0.7 nL. Hence, variation trends of droplet volume in the numerical simulation are consistent with the counterparts of experimental results. The results of numerical simulation show that the discrete volume has less variation with flow rate when the gap is smaller. Observed from the simulation results, the liquid under the membrane

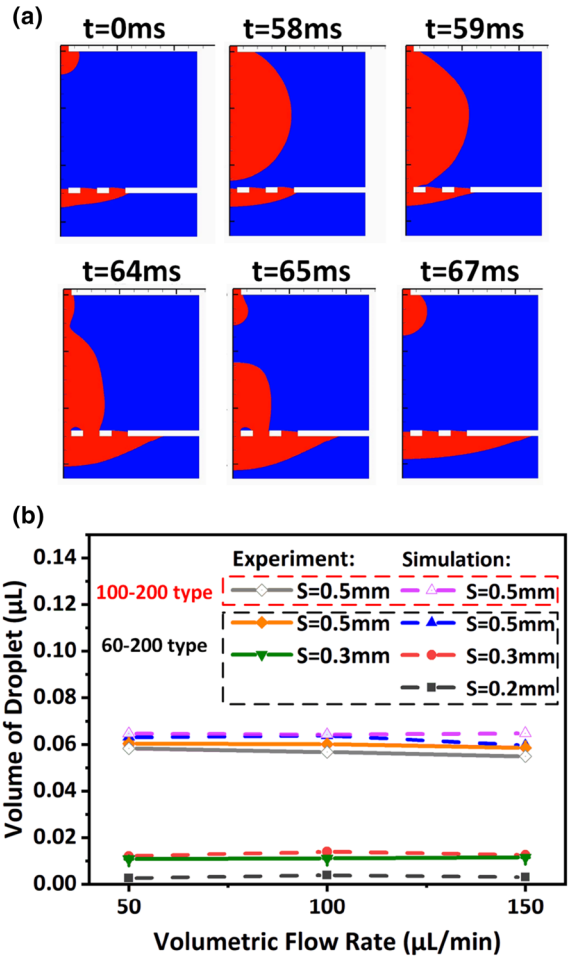

Fig. 4 **a** The images of the droplet discretization process simulated using the DIIB method. In the model, the flow rate, the diameter of the nozzle and the gap distance is set as 50 μL/min, 60 μm and 0.5 mm. **b** The relationship between droplet volume and volumetric flow rate from the simulation and experiment

is fluctuating during the droplet separation. It may be the cause of the volume variation which can be reduced by removing the liquid on the bottom surface in time. Additionally, the deviations between experiment and simulation are 1.8 nL ($S = 0.3$ mm) and 2.4 nL ($S = 0.5$ mm), which may be induced by the size inaccuracy of the gap manipulated manually. Calculated from the propagation of error formula (Coleman and Steele 2009) and Eq. (5), the theoretical random errors of discrete volume are ± 1.5 nL and ± 4.0 nL with the resolution of the manual stage of ± 0.01 mm. Therefore, it can be concluded that smaller gap makes smaller size droplet and less fluctuations of discrete volume as flow rate changes, which confirms the theory and experimental results aforementioned that smaller gap would produce smaller droplets and has higher volume stability.

3.3 Influence of the microporous array

As described in the mathematical model, the Janus membrane plays a significant role in droplet discretization process. In this part, we analyzed the discretization process using different diameters of micropores and pitches of array in the Janus membrane to optimize the structure of array. Here, we experimentally investigated the influences of the pore size and density on the discretized droplet volume. There are three types of Janus membranes explored in the experiment: 100–200 type, 60–200 type, and 60-single type, referring to Janus membranes which have pore diameter of 100 μm and pitch of 200 μm, pore diameter of 60 μm and pitch of 200 μm, and only one pore with diameter of 60 μm, respectively. When the gap distance is set as 0.5 mm and the flow rate is 50 μL/min, the volume of the droplet discretized by TSS of 100–200 type and 60–200 type is 58.3 nL and 60.3 nL, respectively. Considering the volumetric error induced by the displacement inaccuracy, it can be said that the discrete volume is independent of the microporous array. However, as for TSS of 60-single type, the discretization effect shows a quite different process. The liquid accumulates between two superhydrophobic surfaces, and the droplet discretization cannot be performed normally because of the low permeate rate of single-pore Janus membrane, which indicates that the permeate time may dominate the discretization performance of microporous array.

Specifically, we simulated different diameter of micropores and pitch of array in the Janus membrane to predict the optimal structure of array. During the discretization process, the time of absorption (t_m) is highly related to the wettability and the geometric parameters of micropores of Janus membrane. So here we simulated the effects of Janus membrane structure on absorption time. The permeate time t_m and specific details are shown in Table 1. The initial condition is that a droplet with diameter of 0.3 mm is about to contact the membrane in a velocity of 0.0368 m/s which is calculated by $Q/2a_s$ (a_s is the surface area of droplet sphere, Q is the flow rate). The terminal condition is that all liquid penetrated into the lower side of the membrane. So t_m is referring to the period from the initial condition to the terminal condition. Figure 5 shows the simulation results with different

Table 1 Simulation results with different parameters of the microporous array of the Janus

Pores diameter (μm)	Array pitch (μm)	t_m (ms)
60	Single	145.5
60	100	11.75
60	200	35.5
100	Single	55.5
100	200	20.5

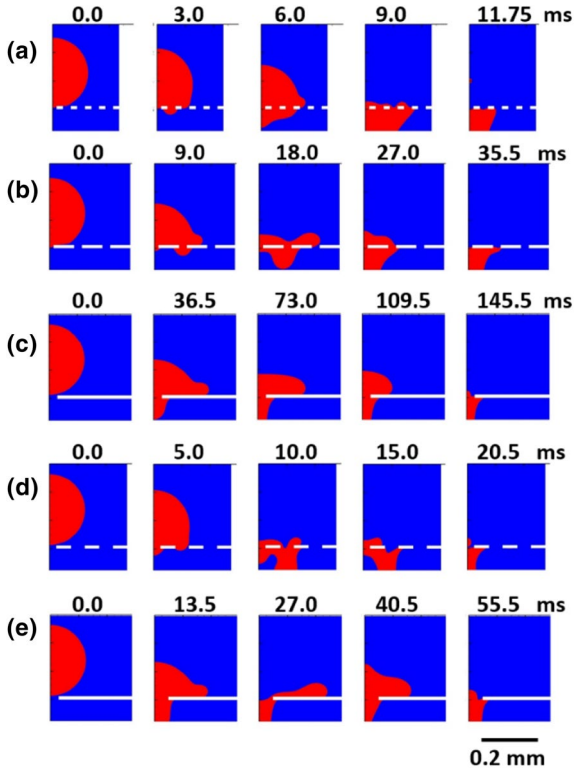

Fig. 5 The process of the droplet merging into the Janus membrane in different array structure parameters: **a** diameter of 60 μm, space of 100 μm; **b** diameter of 60 μm, space of 200 μm; **c** single micropore with diameter of 60 μm; **d** diameter of 100 μm, space of 200 μm; **e** single micropore with diameter of 100 μm

Janus. We noticed that the quickest permeate process takes 11.75 ms to complete when the Janus has pores in a diameter of 60 μm and array pitch of 100 μm. And the longest time is 145.5 ms when the diameter of pore is 60 μm with only one micropore. It reveals that the greater the proportion of porous diameter over array pitch, the faster of the liquid penetrating through the membrane. Shorting the time of permeate is of importance because it means a higher frequency of discretization, indicating a higher flow rate condition that TSS can be served for.

4 Digital flow rate sensor based on isovolumetric discretization effect

The isovolumetric discretization effect demonstrates that droplet size is independent of the flow rate and can be regulated by the TSS, which indicates a potential application in flow metering with controllable resolution. The theory of flow rate (Q) measurement through the TSS can be obtained by $Q = V \cdot f$, where V is the volume of the single discrete droplet, f is the frequency of discretization. Accordingly, the flow rate can be obtained by two simple

detecting steps: firstly, calibrate the discrete volume in advance and then detect the dropping frequency in real time. Then, the volumetric flow rate would be measured by multiplying V and f together. When the constant flow pump is turned on, the flow meter system starts counting and timing the drops. By simply controlling the structure parameter S (distance between two superhydrophobic surfaces), the flowmeter can easily measure flow rate at different resolutions without the changing pipes or apply other extra energy.

The experimental realization and signal detection of TSS-based flowmeter are preliminarily demonstrated. The durations between two droplets are uniform when the flow rate and the gap are constant, indicating the uniformity of every single droplet (Shown in Fig. 6a). At gap of 0.5 mm, when the flow rate is increased from 100 µL/min to 200 µL/min, the duration between two neighboring pulses is reduced by half. Moreover, the frequency is almost proportional to the flow rate in the explored range with the linear regression correlation coefficient (r) of 0.997. It worth noting that liquid may flow from the top to the bottom when the droplet contacts both superhydrophobic layers, which could cause the discrete volume to vary with the flow rate. The connect time can be reflected by the high-level duration shown in Fig. 6a. For example, the high-level duty cycle is about 5.0% of the total cycle when the high-level duration is 1.44 ms and cycle length is 28.7 ms under flow rate of 100 µL/min. And this electrical result corresponds with image data in Fig. 1c where the droplets contact time of the first and second layers is about 4.1% of the total dispersion process time. Speeding up the penetrating can shorten the connect time, which will help to reduce the sensor's system error. Alternately, a calibration of discrete droplet volume in advance is helpful to further improve the precision of the TSS sensor.

5 Conclusions

We reported a novel digital flow rate sensor based on isovolumetric discretization effect using a three-supersurface structure (TSS). The liquid can be truncated in the space between two superhydrophobic surfaces to achieve a consistent discrete volume of liquid in the air under different flow rates. Moreover, the TSS has the ability to adjust the discrete unit volume range by conveniently changing the distance between the two super hydrophobic surfaces rather than applying additional energy. Mathematical model and numerical simulations of the discrete process were also established to further analyze the influences of fluid rate and gap on the volume of discrete elements. The results demonstrated that the frequency of droplet discretization is linearly related to the flow rate. Additionally, the resolution and dynamic range of measurement are tunable by simply adjusting the structural gap of TSS. The developed digital droplet device shows a feasible application on measurement of low flow rate liquid. Due to the advantages of miniaturization and low-cost of TSS-based flowmeter, it is possible to integrate the TSS-based flow rate sensor with some disposable medical supplies to monitor the reagent flow for one-time use, such as the Murphy drip. It can also be used to precisely control the dose of insulin or epinephrine used for the patients in the ICU (Hovorka 2006; Marwitz et al. 2019). Besides, the TSS, serving as a new way of discretizing micro/nanoliter droplets, may stimulate creative inspiration in the field of wearable microfluidic devices for analyzing sweat components, measuring sweat rate and monitoring human health if it expands the material to more flexible and biocompatible polymer material (Bandodkar et al. 2019). In summary, this study provides potential development for smart microfluidic devices with disposable flow rate sensor, which may be applied in future clinical and wearable apparatuses.

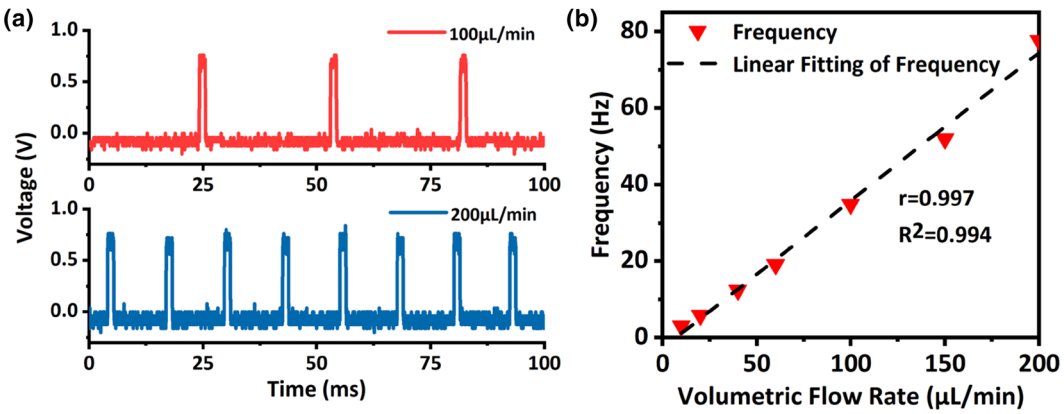

Fig. 6 **a** Continuous recording of the voltage value of the droplet counting circuit over time with the flow rates of 100 µL/min and 200 µL/min with gap of 0.5 mm. **b** The relationship between velocity and frequency of acquisition signal (color figure online)

6 Supplementary materials

Please see supplementary materials for detailed descriptions of the approaches used for the experiments and analysis.

Acknowledgements This research work has been supported in part by the National Natural Science Foundation of China (No. 51675505), the Joint Research Fund for Overseas Chinese, Hong Kong and Macao Young Scientists of the National Natural Science Foundation of China (Grant No. 51628502).

References

Bandodkar AJ et al (2019) Battery-free, skin-interfaced microfluidic/electronic systems for simultaneous electrochemical, colorimetric, and volumetric analysis of sweat. Sci Adv 5:eaav3294. https://doi.org/10.1126/sciadv.aav3294

Ben-Tzvi P, Rone W (2010) Microdroplet generation in gaseous and liquid environments. Microsyst Technol 16:333–356. https://doi.org/10.1007/s00542-009-0962-7

Cao M et al (2015) Superhydrophobic "pump": continuous and spontaneous antigravity water delivery. Adv Funct Mater 25:4114–4119. https://doi.org/10.1002/adfm.201501320

Cataldo A, Cannazza G, Giaquinto N, Trotta A, Andria G (2012) Microwave TDR for real-time control of intravenous drip infusions. IEEE Trans Instrum Meas 61:1866–1873. https://doi.org/10.1109/tim.2012.2192346

Chen H, Liu H-R, Lu X-Y, Ding H (2018) Entrapping an impacting particle at a liquid–gas interface. J Fluid Mech 841:1073–1084. https://doi.org/10.1017/jfm.2018.134

Coleman HW, Steele WG (2009) Experimentation, validation, and uncertainty analysis for engineers, 4th edn. Wiley, Hoboken

Dong Z, Ma J, Jiang L (2013) Manipulating and dispensing micro/nanoliter droplets by superhydrophobic needle nozzles. ACS Nano 7:10371–10379. https://doi.org/10.1021/nn4048099

Droplet Generation (2008) In: Li D (ed) Encyclopedia of microfluidics and nanofluidics. Springer, Boston, p 423. https://doi.org/10.1007/978-0-387-48998-8_367

Francis J, Stamper I, Heikenfeld J, Gomez EF (2018) Digital nanoliter to milliliter flow rate sensor with in vivo demonstration for continuous sweat rate measurement. Lab Chip 19:178–185. https://doi.org/10.1039/c8lc00968f

Heikenfeld J et al (2018) Wearable sensors: modalities, challenges, and prospects. Lab Chip 18:217–248. https://doi.org/10.1039/C7LC00914C

Hillman MR (1989) The prediction of drop size from intravenous infusion controllers. J Med Eng Technol 13:166–176. https://doi.org/10.3109/03091908909044341

Hovorka R (2006) Continuous glucose monitoring and closed-loop systems. Diabet Med 23:1–12. https://doi.org/10.1111/j.1464-5491.2005.01672.x

Liu H-R, Ding H (2015) A diffuse-interface immersed-boundary method for two-dimensional simulation of flows with moving contact lines on curved substrates. J Comput Phys 294:484–502. https://doi.org/10.1016/j.jcp.2015.03.059

Liu H-R, Gao P, Ding H (2017) Fluid–structure interaction involving dynamic wetting: 2D modeling and simulations. J Comput Phys 348:45–65. https://doi.org/10.1016/j.jcp.2017.07.017

Mao Y, Pan Y, Li X, Li B, Chu J, Pan T (2018) High-precision digital droplet pipetting enabled by a plug-and-play microfluidic pipetting chip. Lab Chip. https://doi.org/10.1039/c8lc00505b

Marwitz KK, Giuliano KK, Su W-T, Degnan D, Zink RJ, DeLaurentis P (2019) High-alert medication administration and intravenous smart pumps: a descriptive analysis of clinical practice. Res Social Adm Pharm. https://doi.org/10.1016/j.sapharm.2019.02.007

Murphy JB (1909) Proctoclysis in the treatment of peritonitis. J Am Med Assoc LII:1248–1250. https://doi.org/10.1001/jama.1909.25420420028003a

Ryoun Youn J, Seok Song Y (2012) Cell-encapsulating droplet formation and freezing. Appl Phys Lett 101:133701. https://doi.org/10.1063/1.4754611

Tian X, Jin H, Sainio J, Ras RHA, Ikkala O (2014) Droplet and fluid gating by biomimetic Janus membranes. Adv Funct Mater 24:6023–6028. https://doi.org/10.1002/adfm.201400714

Wood MJ, Aristizabal F, Coady M, Nielson K, Ragogna PJ, Kietzig A-M (2018) The precise and accurate production of millimetric water droplets using a superhydrophobic generating apparatus. Phys Fluids 30:027104. https://doi.org/10.1063/1.5009929

Wu L, Li G-P, Xu W, Bachman M (2006) Droplet formation in microchannels under static conditions. Appl Phys Lett 89:144106. https://doi.org/10.1063/1.2358857

Yang Y, Xing S, Fang Z, Li R, Koo H, Pan T (2017) Wearable microfluidics: fabric-based digital droplet flowmetry for perspiration analysis. Lab Chip 17:926–935. https://doi.org/10.1039/c6lc01522k

Yin K, Ja Duan, Sun X, Wang C, Luo Z (2015) Formation of superwetting surface with line-patterned nanostructure on sapphire induced by femtosecond laser. Appl Phys A 119:69–74. https://doi.org/10.1007/s00339-014-8957-3

Yong J, Chen F, Yang Q, Hou X (2015) Femtosecond laser controlled wettability of solid surfaces. Soft Matter 11:8897–8906. https://doi.org/10.1039/C5SM02153G

Yun J, Khan FA, Baik S (2017) Janus graphene oxide sponges for high-purity fast separation of both water-in-oil and oil-in-water emulsions. ACS Appl Mater Interfaces 9:16694–16703. https://doi.org/10.1021/acsami.7b03322